

How strong are the Rossby vortices?

H. Meheut^{1,2*}, R.V.E. Lovelace³ and D. Lai³

¹*Physikalisches Institut & Center for Space and Habitability, Universität Bern, 3012 Bern, Switzerland*

²*CEA, Irfu, SAp, Centre de Saclay, F-91191 Gif-sur-Yvette, France*

³*Department of Astronomy, Cornell University, Ithaca, NY 14853, USA*

3 March 2022

ABSTRACT

The Rossby wave instability, associated with density bumps in differentially rotating discs, may arise in several different astrophysical contexts, such as galactic or protoplanetary discs. While the linear phase of the instability has been well studied, the nonlinear evolution and especially the saturation phase remain poorly understood. In this paper, we test the non-linear saturation mechanism analogous to that derived for wave-particle interaction in plasma physics. To this end we perform global numerical simulations of the evolution of the instability in a two-dimensional disc. We confirm the physical mechanism for the instability saturation and show that the maximum amplitude of vorticity can be estimated as twice the linear growth rate of the instability. We provide an empirical fitting formula for this growth rate for various parameters of the density bump. We also investigate the effects of the azimuthal mode number of the instability and the energy leakage in the spiral density waves. Finally, we show that our results can be extrapolated to 3D discs.

Key words: accretion, accretion discs - hydrodynamics - instabilities.

1 INTRODUCTION

Understanding the evolution of accretion discs is important for several astrophysical applications. The Rossby wave instability (RWI) (Lovelace et al. 1999) and Rossby vortices it form have been discussed in a large variety of disc systems, from large-scale galactic discs (Lovelace & Hohlfeld 1978; Sellwood & Kahn 1991) and the Galactic centre (Tagger & Melia 2006), to discs in microquasars (Lovelace et al. 2009) and protoplanetary discs (Varnière & Tagger 2006; Meheut et al. 2012). The latter are of particular importance since Rossby vortices may accelerate planetesimal formation. The RWI operates around the density bumps or vortensity bumps (see Section 2) in the disc. In the linear theory, the growth rate of the instability can be computed as an eigenvalue problem. This was done by Li et al. (2000) for 2D discs, by Umurhan (2010) in the shallow water approximation, and by Meheut et al. (2012) and Lin (2012) for 3D vertically stratified discs. After the linear phase, the instability saturates and the linear theory breaks down. The saturation amplitude of the instability is of importance in the several applications. For example, in protoplanetary discs, the vortices formed by the RWI can concentrate the solid particles and hence accelerate the formation of planetesimals. The amplitude of the vortices is a key parameter that determines the amount of solids that

can be concentrated and the size of the resulting planetesimals (Meheut et al. 2012). The Rossby vortices can also influence planet migration in the disc in the latter stage of planet formation (Koller et al. 2003), and the amplitude of migration is determined by the strength of the vortices. In the RWI model of Quasi-Periodic Oscillations (QPO) in microquasars, the saturation amplitude of the RWI is of importance for the understanding of the observed QPO amplitude.

The saturation mechanism of the RWI was already discussed in Li et al. (2001), but no criterion for saturation was given. In this paper, we interpret the growth of the instability in term of particle-wave interaction and use classical plasma physics results in this context, which give the non-linear saturation condition as proposed by Lovelace et al. (2009). In section 2, we present the physical interpretation of the growth of the instability and the model for the saturation mechanism. The numerical simulations are presented and compared with the model in section 3. We then summarise and conclude in the last section.

2 THE RWI

2.1 Linear growth

The RWI can be seen as an equivalent of the Kelvin-Helmholtz instability in differentially rotating discs, and has a similar instability criterion: an extremum in the quantity

* E-mail: heloise.meheut@cea.fr

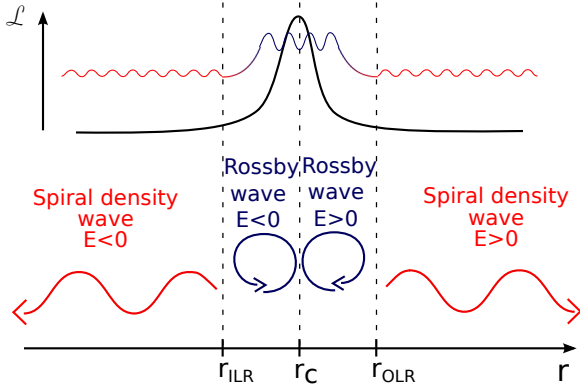


Figure 1. Schematic view of the RWI with the two propagating regions for the Rossby waves and density waves, and in between the evanescent regions. At the corotation radius r_c the wave pattern frequency matches the orbital frequency (Eq. 4). The inner and outer Lindblad radii, r_{ILR} and r_{OLR} , are defined by Eq. (5)

\mathcal{L} related to the vorticity of the equilibrium flow. In a non-magnetised thin disc, this quantity can be written as

$$\mathcal{L} = \frac{\Sigma\Omega}{\kappa^2} (p\Sigma^{-\gamma})^{2/\gamma} = \frac{\Sigma}{2(\vec{\nabla} \times \vec{v})_z} (p\Sigma^{-\gamma})^{2/\gamma}, \quad (1)$$

where Σ is the surface density, \vec{v} the velocity of the fluid, γ the adiabatic index, Ω the rotation frequency, and $\kappa^2 = 4\Omega^2 + 2r\Omega\Omega'$ the squared epicyclic frequency (so that $\kappa^2/2\Omega$ is the vorticity). Here the prime denotes a radial derivative. For barotropic discs considered in this paper, the quantity \mathcal{L} reduces to

$$\mathcal{L} = \frac{\Sigma\Omega}{\kappa^2} = \frac{\Sigma}{2(\vec{\nabla} \times \vec{v})_z}, \quad (2)$$

corresponding to 1/2 of the inverse vorticity¹.

In a disc with such an extremum, two standing Rossby waves can coexist, one on each side of the extremum. We recall here that Rossby waves are vorticity waves propagating on the gradient of vorticity, and their dispersion relation is given by

$$\tilde{\omega} = -\frac{2\kappa^2 c_s^2}{c_s^2(k_r^2 + m^2/r^2) + \kappa^2} \frac{m\mathcal{L}'}{r\Sigma} \quad (3)$$

where ω is the wave frequency, $\tilde{\omega} \equiv \omega - m\Omega$ is the wave frequency in the rotating frame, m and k_r its azimuthal and radial wave numbers, and c_s is the sound speed. The wave corotation radius r_c is defined by:

$$\tilde{\omega}(r_c) \equiv \omega - m\Omega(r_c) = 0. \quad (4)$$

Thus, with the negative gradient of the disc rotation velocity, we have $\tilde{\omega}_{r>r_c} < 0$ and $\tilde{\omega}_{r<r_c} > 0$. From the dispersion relation, one can see that Rossby waves propagate only in the region where $\mathcal{L}' > 0$ if $r < r_c$ and where $\mathcal{L}' < 0$ if $r > r_c$.

We consider here the case of a maximum of \mathcal{L} as plotted in Fig. 1. The wave located in the positive gradient of \mathcal{L} ($r < r_c$) has the pattern frequency smaller than the disc rotation frequency ($\omega/m < \Omega$) and carries negative energy

(i.e., increasing wave amplitude tends to remove energy from the fluid). On the other hand, the wave in the negative gradient of \mathcal{L} has $\omega/m > \Omega$ and carries positive energy. The growth of the RWI is due to the interaction between the two Rossby waves with respectively positive and negative energies. The total energy is conserved while the wave amplitude increases. The mechanism for the growth of the instability is then localised in the corotation region and does not depend on the boundary conditions.

As explained by Tagger (2001), in accretion discs the differential rotation couples Rossby waves to density waves. These density waves can only propagate outside the two (inner and outer) Lindblad resonances radii r_{LR} defined as

$$\omega - m\Omega(r_{\text{LR}}) = \pm\kappa(r_{\text{LR}}). \quad (5)$$

Between the two propagation zones the wave is evanescent and tunnelling is possible as plotted in Fig. 1. As detailed in Tsang & Lai (2008) and Lai & Tsang (2009), these propagation regions clearly appear when expressing the linearized perturbation equations in the form of Schrödinger equation, with the effective potential given by

$$V_{\text{eff}} = \frac{2m\Omega}{r\tilde{\omega}} \frac{d}{dr} \left(\ln \frac{\Omega\Sigma}{\kappa^2 - \tilde{\omega}^2} \right) + \frac{m^2}{r^2} + \frac{\kappa^2 - \tilde{\omega}^2}{c_s^2}. \quad (6)$$

The waves are propagating in the region where $V_{\text{eff}}(r)$ is negative and evanescent where $V_{\text{eff}}(r)$ is positive. This effective potential is plotted in Fig. 2 for the specific configuration considered below.

2.2 Non-linear saturation

To estimate the amplitude at which the linear calculation stops to be valid, we use a standard plasma criterion which gives, for instance, the breakdown of the Landau damping theory due to particle trapping (O’Neil 1965; Krall & Trivelpiece 1973). We consider a fluid particle in a Rossby wave with the vorticity amplitude ω_v exponentially growing with time during the linear stage,

$$|\omega_v| \propto \exp(\gamma t). \quad (7)$$

We here use the convention to express time in units of Ω_0^{-1} .

The estimation of the rotation time of a fluid particle in a vortex is related to the vorticity. For instance for a circular vortex with constant vorticity, it can be estimated as

$$\tau_T \sim 4\pi/|\omega_v|. \quad (8)$$

However in the case of the vortices formed by the RWI, the vortex doesn’t have an analytical expression and the turnover timescale can not be computed analytically. From the simulations presented in the next section, we estimated

$$\tau_T \sim 2/|\omega_v|. \quad (9)$$

This circular motion around the vortex centre is a major perturbation to the circular orbit of the fluid particle around the disc centre and it modifies the radial structure of the disc in the region of the vortices on a time scale τ_T . The linear calculation of the growth of the Rossby wave instability is determined by this radial structure of the disc and especially by the radial structure of \mathcal{L} . Therefore, this linear approach

¹ Vortensity is defined as the ratio of vertical vorticity to surface density: $\frac{(\vec{\nabla} \times \vec{v})_z}{\Sigma}$

is only valid when the growth timescale ($1/\gamma$) is smaller than τ_T . This occurs when

$$\frac{|\omega_v|}{2} \sim \gamma. \quad (10)$$

In other words, the exponential growth of the wave amplitude necessarily ends when the fluid particle motion in the vicinity of resonant radius r_c differs appreciably from the strictly azimuthal motion in the equilibrium. Note that the saturation criterion (10) is only order-of-magnitude, and similar criterion was proposed by Lovelace et al. (2009) in a different context. Below we perform non-linear numerical simulations to calibrate this criterion.

3 NON-LINEAR SIMULATIONS

3.1 Methods

We have performed two dimensional (2D) non-linear simulations of a differentially rotating disc with a constant surface density except for a Gaussian bump. This over-density gives an extremum of \mathcal{L} in which the instability can grow.

We work in cylindrical coordinates (r, φ) with the 2D Euler equations

$$\partial_t \Sigma + \vec{\nabla} \cdot (\rho \vec{v}) = 0, \quad (11)$$

$$\partial_t (\Sigma \vec{v}) + \vec{\nabla} \cdot (\vec{v} \Sigma \vec{v}) + \vec{\nabla} p = -\Sigma \vec{\nabla} \Phi_G, \quad (12)$$

where Σ is the surface density of the fluid, \vec{v} its velocity, and p its pressure. $\Phi_G = -GM_*/r$ is the gravitational potential of the central object with G the gravitational constant and M_* the mass of the star. We consider a *globally* isothermal flow, i.e. with a radially constant sound speed, and a linear relation between pressure and density $p = c_s^2 \Sigma$.

The initial surface density, normalized to Σ_0 is given by

$$\Sigma/\Sigma_0 = 1 + \chi \exp\left(-\frac{(r-r_0)^2}{2\sigma^2}\right). \quad (13)$$

Our canonical parameters are $r_0 = 1.$, the amplitude of the bump χ is chosen in the range $[0.15, 0.3]$, and its width is given by $\sigma/r_0 = 0.05$. Although we will also present results for different values of σ/r_0 . The disc scale height is fixed to $h = c_s/\Omega_0 = 0.1r_0$, Ω_0 being the Keplerian orbital frequency at r_0 . The initial azimuthal velocity is chosen to achieve radial equilibrium. A low amplitude perturbation is added to this equilibrium:

$$v_r = \epsilon \sin(m\phi) \exp\left(-\frac{(r-r_0)^2}{2\sigma^2}\right) \quad (14)$$

with $\epsilon = 10^{-4}$ and the azimuthal mode number $m \in [2, 5]$. We have also performed simulations with initial random perturbations of the same amplitude.

We use the Message Passing Interface-Adaptive Mesh Refinement Versatile Advection Code (MPI-AMRVAC) (Keppens et al. 2012), with a uniform grid. The numerical scheme is the Total Variation Diminishing Lax-Friedrich scheme (see Tóth 1996) with a third order accurate Koren limiter (Koren 1993) on the primitive variables. We use a uniform cylindrical grid with $r/r_0 \in [0.2, 2.4]$, and the full azimuthal direction $\varphi \in [0, 2\pi]$. Numerical convergence has been tested and two different resolutions have been used: (1024, 128) for most of the simulations ($m = 1$ to 4) but

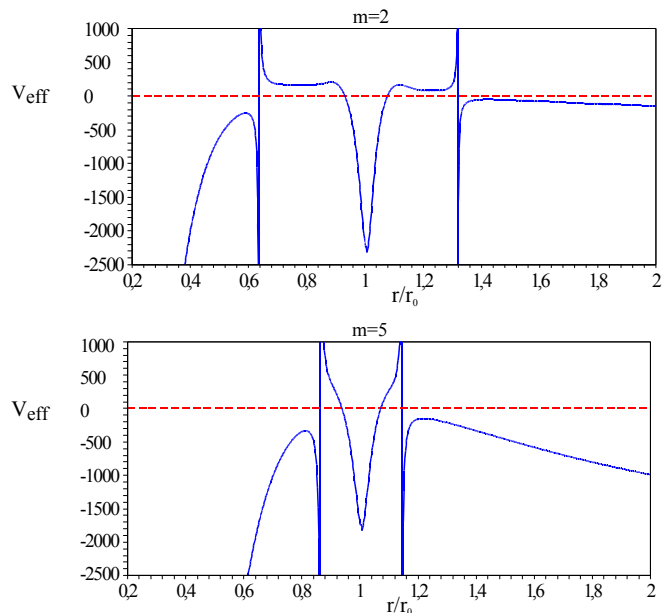


Figure 2. Effective potential for a density profile given by Eq. 13 with $\chi = 0.2$ for $m = 2$ (upper panel) and $m = 5$ (lower panel). Waves can propagate only in the regions where $V_{\text{eff}}(r) < 0$.

a resolution of (1024, 256) was needed for the highest azimuthal modes number $m = 5$ and the simulations with white noise perturbations. There is a null radial velocity at the inner and outer boundary of the grid.

This numerical configuration is very similar to the one of Meheut et al. (2012) which has proven to accurately describe the instability, with a very good agreement with the analytical approach in the linear phase. For all these simulations, the square of the epicyclic frequency, κ^2 , is positive at all radii and the disc is stable against axisymmetric perturbations.

3.2 Results

For each of the 20 simulations, the linear growth rate of the instability is obtained by fitting the amplitude of the vorticity in the Rossby waves region as a function of time (see Fig. 3). We have previously shown that this method gives growth rate very similar to the one obtained by solving the linear equations (Meheut et al. 2012). The amplitude of the waves initially grows exponentially until saturation. As explained in section 2.2, we estimate saturation to arise when the waves reach a vorticity of the order of 2γ . This amplitude is plotted as a dashed line in Fig. 3.

For each simulation, the ratio of the maximum of vorticity to the expected value, $\omega_v^{max}/2\gamma$, is given. The saturation amplitude reached in the non-linear numerical simulations for $m = 4$ and $m = 5$. Similar to the non-linear evolution of the Landau damping, we also obtain oscillations in the waves amplitude.

For low mode numbers, the maximum vorticity is slightly below the estimation. This is due to the shape of the vortices. Indeed the vortices with low m have elongated shapes as can be seen in Fig. 4 where vortices streamlines in the (r, φ) plane are plotted. These streamlines are computed with the perturbed velocity during the linear stage of the

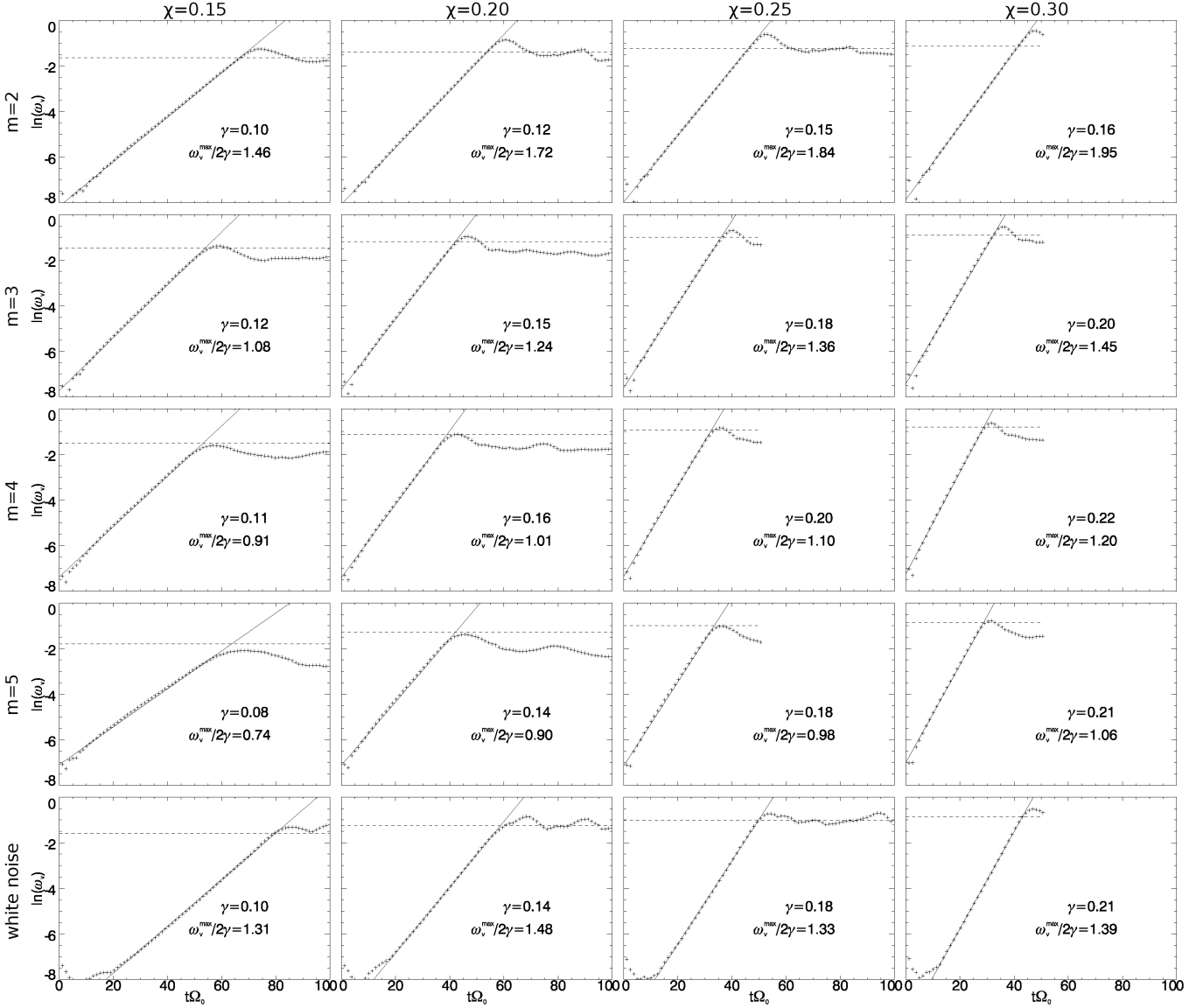


Figure 3. Amplitude of the Rossby waves (vorticity) on logarithmic scale as a function of time (in units of Ω_0^{-1}). A fit of the exponential growth (solid line) gives the growth rate γ . The dashed line corresponds to the saturation amplitude estimated by the model.

instability. To allow for a comparison between different m cases, the time slices for these plots are chosen such that the perturbations have about the same amplitudes. This shape was to be expected as the width of the Rossby wave propagation region is fixed by the width of the initial density bump and the length of the vortices is directly related to the azimuthal mode number m . Assuming a doubled circulation time for the elongated $m = 2$ vortices gives the correct saturation amplitude, as one can see in Fig. 3 for the $[m = 2, \chi = 0.30]$ simulation.

On the other hand, the vorticity maximum is overestimated for the highest azimuthal mode number when the growth rate is low. See for instance the $[m = 5, \chi = 0.15]$ simulation. We have checked that this is not related to numerical dissipation by doubling the resolution and obtaining no modification of ω_v^{\max} . Indeed the energy loss responsible for the low saturation amplitude may be due to the

density waves propagating outside the Lindblad resonances that were not considered in the local mechanism proposed for growth and saturation in section 2.2. The amplitude of the density waves and the energy loss is the highest when the Lindblad resonances are close to the corotation radius and the width of the evanescent wave region is small. This regions correspond to a positive effective potential V_{eff} in Fig. 2. Since the Lindblad resonances are closer to corotation for higher azimuthal mode number, the evanescent region is narrower. Energy transmission through this region is then carried away by density waves. These density waves can then become non-linear when they reach high amplitudes. This may explain the lower amplitude at saturation. Moreover these density waves are also responsible for the angular momentum transfer through the disc and as a result for the evolution of the radial structure of the disc from which the linear growth is computed. The distance between the two

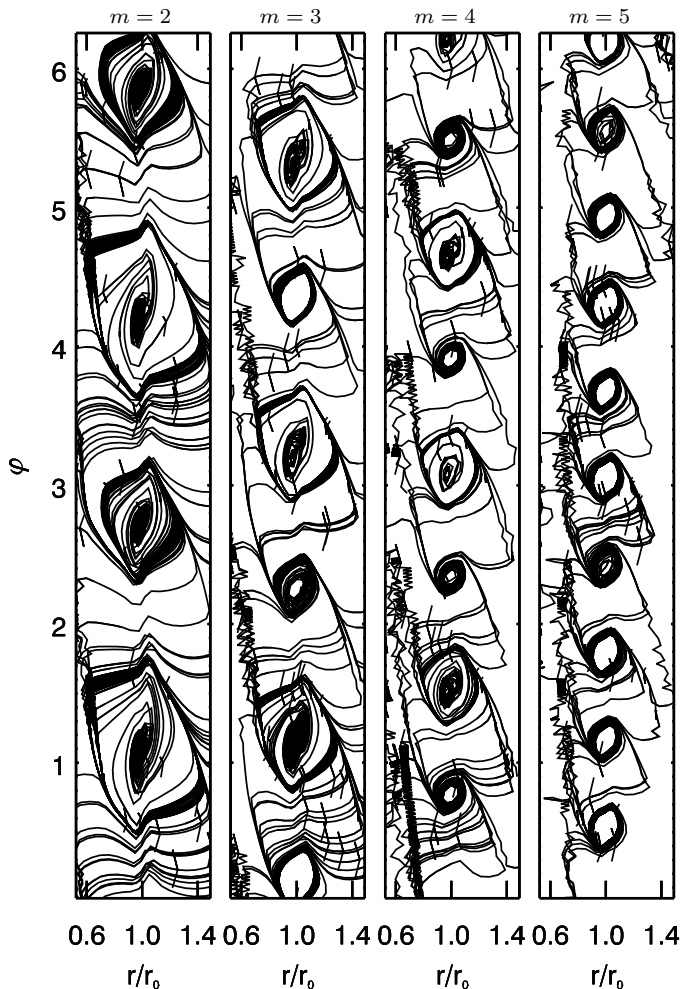


Figure 4. Streamlines showing the shape of the vortices for the four azimuthal mode numbers considered here. For the lowest mode number the vortices are elongated, for the highest ones the vortices are circular.

propagation region appears clearly on Fig. 5 where both the vorticity waves in the region of corotation and the position of the Lindblad resonances are visible. One can also identify the spiral density waves propagating inwards and outwards from the Lindblad resonances in the $m = 5$ plot. To further check the importance of the Lindblad resonances, we have performed numerical simulations with a shallower density bump ($\sigma/r_0 = 0.4$) but with the same azimuthal mode number $m = 5$. The density bump being shallower, the Lindblad resonances are situated further away from the vortices and less energy is lost in the spirals waves. Fig. 6 shows that in this case the saturation amplitude is correctly estimated.

The amplitude of saturation in the simulations with an initial white noise perturbation is more complex. Multiple modes grow simultaneously in the linear phase with different growth rates, as can be seen on Fig. 7. However we still obtain an exponential growth of the total perturbation as the growth rates of the different modes are similar. The growth rate of the total perturbation ($0.21\Omega_0$) is slightly smaller than the highest growth rate of the different modes ($0.22\Omega_0$ for $m = 4$) due to this coexistence of multiple modes with

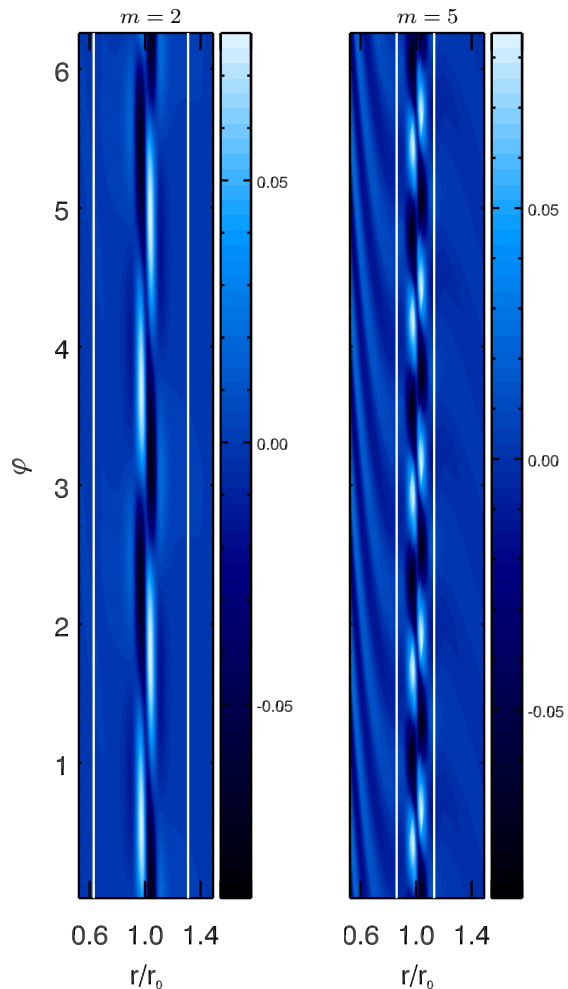


Figure 5. Vorticity (Ω_0) of the flow near corotation for $m=2$ and $m=5$. The white lines show the position of the Lindblad resonances. The width of the evanescent region between the vorticity wave and the Lindblad resonance is larger for lower m .

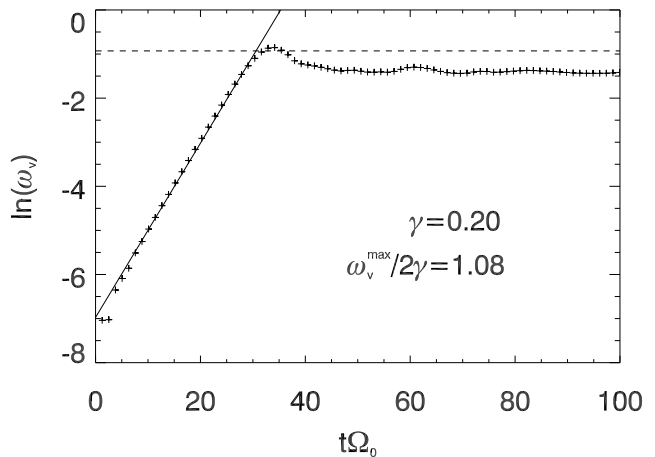


Figure 6. Amplitude of the Rossby waves (vorticity) on logarithmic scale as a function of time (in units of Ω_0^{-1}) for the simulation with $\sigma/r_0 = 0.4$ and $m = 5$. A fit of the exponential growth (solid line) gives the growth rate γ . The dashed line corresponds to the saturation amplitude estimated by the model.

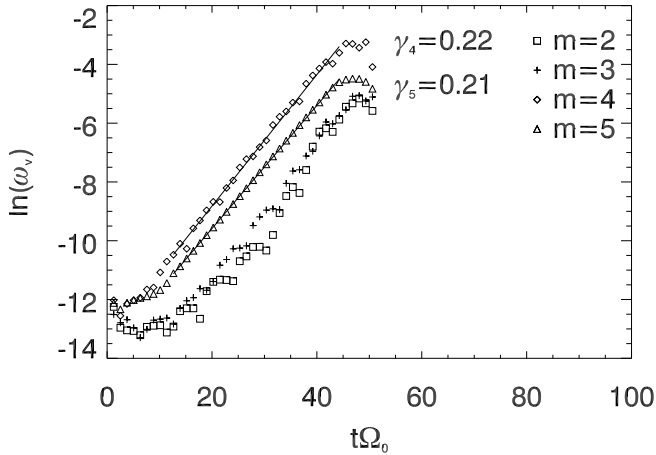


Figure 7. Amplitudes of the Rossby waves with different m 's as a function of time. The simulation starts out with a random white noise, with the parameters $\chi = 0.3$, $\sigma/r_0 = 0.05$, $c_s/(r_0\Omega_0) = 0.1$. The different m component is obtained by a Fourier analysis in the azimuthal direction. The grow rates of the dominant modes are also given.

similar growth rate. These different modes then interact in the non-linear phase, but one can see that eq. (10) still gives a good approximation of the saturation amplitude of the instability in this more realistic case.

3.3 Fitting formula

In order to give an estimation of the growth rate of the instability based on the parameters of the density bump, we performed simulations with initial random perturbations and with $\chi \in [0.1, 0.3]$ and $\sigma/h \in [0.45, 0.6]$. Fitting separately the dependence of the growth rate on χ and σ/h , and then combining, we find that γ is approximately given by

$$\frac{\gamma}{\Omega_0} \simeq \frac{k_1}{(\sigma/h)^{4/3}} \left(\frac{\chi}{\sigma/h} - k_2 \right)^{2/3}, \quad (15)$$

with $k_1 = 0.142$ and $k_2 = 0.138$. Here Ω_0 the Keplerian frequency at the location of the density bump, σ/h and χ specify the width and amplitude of the bump (see eq. 13), and $h = c_s/\Omega_0$ is the disc scale height. Note that this fitting formula should be applied only in the range of parameters specified above and require that the disc be stable against axisymmetric perturbations (i.e., the Rayleigh criterium $\kappa^2 > 0$, is satisfied). Eq. 15 also corresponds to the growth rate of the fastest growing mode ($m \sim 4$) in the linear theory. The amplitude of maximum vorticity at saturation is given by

$$|\omega_v| \sim \frac{2\Omega_0 k_1}{(\sigma/h)^{4/3}} \left(\frac{\chi}{\sigma/h} - k_2 \right)^{2/3}. \quad (16)$$

3.4 3D simulation

In the above we have considered 2D discs, neglecting their vertical structure. Recent study of the RWI in 3D vertically stratified discs has revealed unexpected vertical displacements inside the vortices (Meheut et al. 2010) that could be relevant for the saturation mechanism. However Meheut et al. (2012) and Lin (2012) have shown that the

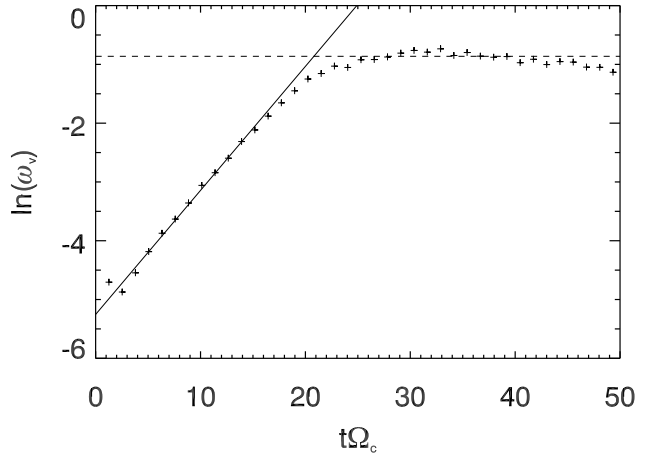


Figure 8. Amplitude of the Rossby waves (mid-plane vorticity) on logarithmic scale as a function of time for the 3D simulation. A fit of the exponential growth gives the growth rate (solid line).

growth rate is only slightly modified (decreased) in a fully stratified disc. Moreover the vertical velocity in the vortices is of low amplitude compared to the radial and azimuthal perturbed velocity. As a result, we do not expect the circulation time to be significantly modified by this vertical circulation. To confirm the relevance of our model for 3D stratified discs, we perform a numerical simulation in such a configuration. We choose $m = 4$ and $\chi = 0.25$, and the volume density is chosen to have a surface density similar to the 2D case (see Meheut et al. 2012). The resulting growth and saturation of the instability is plotted in Fig. 8. The predicted maximum amplitude of the instability is correct, meaning that the model can be extended to 3D discs. This can then be also applied to the saturation phase obtained in Meheut et al. (2012) where the long-term stability of the 3D vortices was studied. After the saturation the vortices continue to evolve, they tend to merge as in an inverse cascade and eventually to decay.

4 SUMMARY

We have tested numerically the non-linear saturation mechanism for the Rossby wave instability proposed by Lovelace et al. (2009). This is based on the classical results of particle-wave interaction well known for unstable electron plasma waves. We have shown that non-linear saturation of the RWI occurs when the trapping frequency of the particles in the Rossby vortices equals the instability growth rate. We have estimated the trapping frequency by the vorticity of the Rossby wave; this is accurate for circular vortices but is only a lower limit for elongated vortices. We also discussed the linear coupling between the Rossby waves and the density waves. This has the effect of decreasing the amplitude of the vorticity wave. Finally, we gave an estimation for the amplitude of the vortices at saturation based on the characteristics of the density bump.

Our paper focused on the non-linear saturation of the linear instability in an initially steady disc. We did not considered the mechanism for the formation of the pressure bump causing the instability. In a disc where the bump is

continuously sustained by some accretion processes, the disc is not steady and a future step is to take into account the evolution of the shape of the bump in the study of the instability.

ACKNOWLEDGMENTS

We thank the referee G. Lesur for his useful comments. This work has been supported in part by NSF grants AST-1008245 and AST-1211061 and the Swiss National Science Foundation. RVEL was partly supported by NASA grant NNX11AF33G.

REFERENCES

- Keppens R., Meliani Z., van Marle A., Delmont P., Vlasov A., van der Holst B., 2012, *Journal of Computational Physics*, 231, 718
- Koller J., Li H., Lin D. N. C., 2003, *ApJL*, 596, L91
- Koren B., 1993, *Notes on numerical fluid mechanics*. Vol. 45 of *A robust upwind discretization method for advection, diffusion and source terms*
- Krall N., Trivelpiece A., 1973, *Principles of plasma physics*. McGraw-Hill
- Lai D., Tsang D., 2009, *MNRAS*, 393, 979
- Li H., Colgate S. A., Wendroff B., Liska R., 2001, *ApJ*, 551, 874
- Li H., Finn J. M., Lovelace R. V. E., Colgate S. A., 2000, *ApJ*, 533, 1023
- Lin M.-K., 2012, *MNRAS*, 426, 3211
- Lovelace R. V. E., Hohlfield R. G., 1978, *ApJ*, 221, 51
- Lovelace R. V. E., Li H., Colgate S. A., Nelson A. F., 1999, *ApJ*, 513, 805
- Lovelace R. V. E., Turner L., Romanova M. M., 2009, *ApJ*, 701, 225
- Meheut H., Casse F., Varniere P., Tagger M., 2010, *A&A*, 516, A31+
- Meheut H., Keppens R., Casse F., Benz W., 2012, *A&A*, 542, A9
- Meheut H., Meliani Z., Varniere P., Benz W., 2012, *A&A*, 545, A134
- Meheut H., Yu C., Lai D., 2012, *MNRAS*, p. 2748
- O’Neil T., 1965, *Physics of Fluids*, 8, 2255
- Sellwood J. A., Kahn F. D., 1991, *MNRAS*, 250, 278
- Tagger M., 2001, *A&A*, 380, 750
- Tagger M., Melia F., 2006, *ApJL*, 636, L33
- Tóth G., 1996, *Astrophysical Letters Communications*, 34, 245
- Tsang D., Lai D., 2008, *MNRAS*, 387, 446
- Umurhan O. M., 2010, *A&A*, 521, A25+
- Varniere P., Tagger M., 2006, *A&A*, 446, L13